Self-assembling peptide-enriched electrospun polycaprolactone scaffolds promote the *h*-osteoblast adhesion and modulate differentiation-associated gene expression

Roberta Danesin [a], Paola Brun [b], Martina Roso [a], Florian Delaunay [c], Valérie Samouillan [c], Katya Brunelli [a], Giovanna Iucci [d], Francesca Ghezzo [a], Michele Modesti [a], Ignazio Castagliuolo [b], Monica Dettin [a,*]

[a] *Department of Industrial Engineering, University of Padua, Via Marzolo 9, 35131, Padua, Italy*
[b] *Department of Molecular Medicine, University of Padua, Via Gabelli 63, 35121, Padova, Italy*
[c] *CIRIMAT UMR 5085, Polymers Physics, Carnot Institute, University Paul Sabatier, 118 route de Narbonne, 31062, Toulouse cedex 09, France*
[d] *Department of Physics "E. Amaldi", University of Roma Tre, Via della Vasca Navale 84, 00146 Roma, Italy*

Keywords:
Self-assembling peptides
Polycaprolactone
RGD
Electrospinning
h-osteoblasts

Electrospun polycaprolactone (PCL) is able to support the adhesion and growth of *h*-osteoblasts and to delay their degradation rate to a greater extent with respect to other polyesters. The drawbacks linked to its employment in regenerative medicine arise from its hydrophobic nature and the lack of biochemical signals linked to it. This work reports on the attempt to add five different self-assembling (SA) peptides to PCL solutions before electrospinning. The hybrid scaffolds obtained had regular fibers (SEM analysis) whose diameters were similar to those of the extracellular matrix, more stable hydrophilic (contact angle measurement) surfaces, and an amorphous phase constrained by peptides (DSC analysis). They appeared to have a notable capacity to promote the *h*-osteoblast adhesion and differentiation process by increasing the gene expression of alkaline phosphatase, bone sialoprotein, and osteopontin. Adding an Arg-Gly-Asp (RGD) motif to a self-assembling sequence was found to enhance cell adhesion, while the same motif condensed with a scrambled sequence did not, indicating that there is a cooperative effect between RGD and 3D architecture created by the self-assembling peptides. The study demonstrates that self-assembling peptide scaffolds are still able to promote beneficial effects on *h*-osteoblasts even after they have been included in electrospun polycaprolactone. The possibility of linking biochemical messages to self-assembling peptides could lead the way to a 3D decoration of fibrous scaffolds.

Introduction

Characterized by both regulatory and structural functions, the extracellular matrix (ECM) is a nanofibrous network of structural proteins, adhesive proteins, and glycosaminoglycans which nature developed as a scaffold for tissue formation. In an effort to mimic ECM, several studies have demonstrated that nanofibrous polymeric or hybrid scaffolds are more similar to ECM than to microfibrous scaffolds [1]. Nanofibrous structures can easily be produced by electrospinning. Biocompatible, FDA-approved, and showing a slower degradation profile with respect to other polyesters such as poly-lactic and poly-glycolic acids, polycaprolactone (PCL) has frequently been used as scaffolding material for bone regeneration. While several studies have demonstrated that PCL is able to support the adhesion and growth of different cell types (i.e. skeletal muscle cells, smooth muscle cells, fibroblasts, chondrocytes, endothelial cells, human mesenchymal stem cells) [2–7], its usefulness in biomedical application would be enhanced if biochemical messages could be linked to it.

Research related to naturally inspired but synthetic low-molecular-weight peptides able to aggregate by self-assembling has also been receiving increasing attention. Self-assembling (SA) peptide hydrogels are nanostructural materials that functionalize easily with chemotactic factors, growth factors or adhesive peptides [8–11] and are able to create suitable environments for culturing cells, triggering tissue regeneration and for releasing drugs. Self-assembling peptide scaffolds have been extensively studied for their potential application in bone-related therapies as biomaterial due to their good bone conduction properties. Compared to Matrigel™, these scaffolds have been shown to be more effective in promoting the bone regeneration of calvaria bone defects in mice [12]. Synthetic materials appear to be effective for small defects, but self-assembling peptide scaffolds seem to be insufficient to regenerate or reconstruct damaged articular cartilage in large load-bearing bones. This work aimed to add self-assembling peptides [13] to a PCL solution to be electrospun in order to assess the potential of modulating the excessive softness of those hydrogels and to add biomimetic molecules to PCL scaffolds. The additional inclusion of hydroxyapatite can significantly enhance the fiber stiffness of electrospun

* Corresponding author. Fax: +39 049 8275555.
E-mail addresses: roberta.danesin@unipd.it (R. Danesin), paola.brun.1@unipd.it (P. Brun), martina.roso@unipd.it (M. Roso), florian.delaunay@gmail.com (F. Delaunay), vsamou@cict.fr (V. Samouillan), katya.brunelli@unipd.it (K. Brunelli), iucci@uniroma3.it (G. Iucci), francesca.ghezzo@unipd.it (F. Ghezzo), michele.modesti@unipd.it (M. Modesti), ignazio.castagliuolo@unipd.it (I. Castagliuolo), monica.dettin@unipd.it (M. Dettin).

http://dx.doi.org/10.1016/j.bone.2012.08.119

scaffolds [14]. This approach will potentially make it possible to create a matrix of PCL fibers with diameters a few hundred nanometers across containing self-assembling peptide fibers whose diameters are 10 times smaller. The physical–chemical and biological characterization of scaffolds produced by electrospinning mixing different synthetic self-assembling peptides [13] to PCL is presented here.

Materials and methods

Peptide synthesis

All peptides were synthesized by solid-phase peptide synthesis (Applied Biosystems Mod 431A, Foster City, CA) using Fmoc chemistry. After being deprotected, the peptides were extensively purified and characterized, as described elsewhere [13]. The sequence and the name of all the peptides used to produce electrospun scaffolds are listed in Table 1. All the peptides were synthesized as C-terminal amides. Abu refers to α-aminobutyric acid. All the sequences follow the typical pattern of ionic complementary peptides and can consequently self-aggregate with the exception of RGD-EAKsc. The varied amino acid compositions of these peptides, however, produce different propensities for β-sheet conformation in solution, and the aggregation capacity depends on the secondary structure [13]. The RGD-EAKsc peptide consists in the RGD cell adhesive sequence condensed to an EAK scrambled sequence. Not, thus, the result of a self-assembled peptide, it is used as a negative control in biological assays. The RGD-EAK peptide is composed by a RGD adhesive motif condensed to the N-terminus of the self-assembling EAK peptide.

Solutions for electrospinning

All solutions were prepared dissolving 10% (wt/wt) of solute in 1,1,1,3,3,3-hexafluorine-2-propanol (HFIP) (Sigma-Aldrich, Milan, Italy). The polymer/peptide solutions were prepared by dissolving 0.2527 g of PCL (Mv 60,000, Sigma-Aldrich) and 0.0133 g of self-assembling peptide in 1.5 mL (2.349 g) of HFIP. A peptide concentration of 1% w/v proximal to ours was utilized in Gelain et al.'s work [15]. A control solution (10% wt/wt) containing only PCL (0.266 g) was also prepared. The solutions were stirred for 3 h to obtain a homogeneous mixture.

Incubation of the PCL/RGD-EAK scaffold with a saline buffered solution

In order to evaluate the secondary structure of the peptide incorporated into the matrix, the PCL/RGD-EAK scaffold was incubated with phosphate buffered saline (150 mM NaCl, 10 mM sodium phosphate, pH 7.4) for 3 days and subsequently washed with MilliQ water and dried under a vacuum for 1 h.

Electrospinning

During the electrospinning process, the solution was released from a 5 mL syringe through a 27G needle at a 1 mL/h flow rate by a volumetric pump; the voltage between the collector and the solution was 16 kV, and the air flow pressure was 0.1 kg/cm^2. Fibers were collected for 1 h on an aluminium foil collector (15 × 15 cm) at a distance of 15 cm from the needle. After deposition all the samples were dried under the vacuum for 1 h in the presence of P_2O_5.

Table 1
The names and sequences of the synthetic peptides.

Abbreviation	Sequence
EAK	A-E-A-E-A-K-A-K-A-E-A-E-A-K-A-K
DAK	A-D-A-D-A-K-A-K-A-D-A-D-A-K-A-K
EAbuK	Abu-E-Abu-E-Abu-K-Abu-K-Abu-E-Abu-E-Abu-K-Abu-K
EYK	Y-E-Y-E-Y-K-Y-K-Y-E-Y-E-Y-K-Y-K
RGD-EAK	R-G-D-A-E-A-E-A-K-A-K-A-E-A-E-A-K-A-K
RGD-EAK sc	R-G-D-A-A-K-A-E-A-E-A-A-E-K-A-K-A-E-K

Scanning electron microscopy

Electrospun scaffolds were sputter coated with carbon (EMITECH K950x Turbo Evaporator, EBSciences, East Granby, CT) and observed under SEM (Cambridge Stereoscan 440 SEM, Cambridge, UK). Images were taken at magnifications of 30,000 Å with an accelerating voltage of 15 kV. The diameter range of the fabricated nanofibers was measured using image analysis software (ImageJ, National Institutes of Health, Bethesda, MD). For each sample, three images at different magnifications and in three different zones of the sample were taken.

Contact angle measurements

Contact angles were measured using a SURFTENS angulometer (OEG, GmbH, Frankfurt, Germany). One sample for each kind of scaffold was set onto a silica slide and a drop of deionized water was deposed for contact angle measurement. The contact angle measurements have been done in triplicate.

Differential scanning calorimetry (DSC)

Thermograms were recorded with a DSC Pyris (Perkin Elmer, San Jose, CA). The temperature and power scales were calibrated following the manufacturer's instructions with cyclohexane and indium as ICTA standards. Samples (2–5 mg) were sealed into aluminum pans and empty pans were used as references. After cooling at 20 °C/min to −100 °C, scans were performed from −100° to 80 °C at 20 °C/min. Additional measurements were taken between 20° and 80 °C at 5 °C/min. DSC thermograms at 10 °C/min were performed in triplicate.

Thermally simulated depolarization currents analysis (TSDC)

Depolarization current measurements were carried out with a dielectric TSCII apparatus (SETARAM Instrumentation, Caluire, France). Samples were placed between two stainless steel electrodes. Before the experiments were begun the cryostat was flushed and filled with dry He to insure good thermal exchanges. To record complex spectra, the sample was polarized with a static electric field E_p at a given polarization temperature T_p for a time t_p which is long enough to reach the equilibrium polarization. The sample was then quenched by a cooling process to $T_0 \ll T_p$, allowing the orientation polarization $P(T_p)$ to be frozen-in. The electric field was finally cut off and the sample was short-circuited for a time t_{cc} long enough to remove fast relaxing surface charges and to stabilize the sample temperature. The capacitor was then connected to a very sensitive electrometer (Keithley 642, 10^{-16} A accuracy). The depolarization current I(T) induced by the linear temperature increase of $(T = qt + T_0)$ was subsequently recorded versus temperature, giving the relaxation spectrum of the sample. In this study, the polarization conditions resulting in reproducible dipolar relaxations were as follows: $T_p = 0$ °C, $t_p =$ 2 min, $E_p = 600$ V/mm, $t_{cc} = 2$ min and $q = 7$ °C/min.

The TSC spectra of hydrated elastin obtained from this procedure are complex arising from a distribution of relaxing entities. The Fractional Polarization (FP) technique was applied in order to resolve these spectra experimentally in a series of elementary depolarizations. The sample was only polarized for this investigation within a narrow temperature window ΔT during the cooling process, and the depolarization current was recorded as described elsewhere. A value of 5 °C was used in the present work for the fractional polarization interval. By shifting the ΔT polarization window by 5 °C steps within the temperature range of the complex relaxation modes, a set of elementary processes was obtained.

X-ray photoelectron spectroscopy

X-ray photoelectron spectroscopy (XPS) investigations were performed using an instrument of our own construction and equipped with a 150 mm mean radius hemispherical electron analyzer and a 16-channel detector. Mg Kα non-monochromatized X-ray radiation ($h\nu = 1253.6$ eV) was used to record peptide (C1s, N1s, O1s) and polymer (C1s, O1s) core-level spectra on the respective samples. The Al2p signal from the Al foil substrate was too low to be detected in any of the samples investigated indicating that there was a thick mat of polymer nanofibers. The spectra were energy referenced to the C1s signal of aliphatic carbons located at a binding energy (BE) of 285.0 eV [16]. The standard deviation on the measured BE values was ± 0.1 eV. Atomic ratios were calculated from the peak intensities with Scofield cross sections. A curve fitting analysis of the C1s, N1s and O1s spectra was performed using Gaussian curves as fitting functions. Measurements were taken on at least two different samples from each scaffold.

FT-IR spectroscopy

Reflection absorption infrared spectra (RAIRS) of the polymer nanofibres deposited onto Al foil were recorded in the 4000–400 cm^{-1} range by means of a VECTOR 22 (Bruker, Billerica, MA) FT-IR interferometer, equipped with a DTGS detector and with a reflectance/grazing angle accessory (Specac, Orpington, UK); the incidence angle of the impinging radiation was 70°. Curve-fitting analysis of the FTIR spectra was performed using Gaussian curves as fitting functions. Measurements were taken on at least two different samples from each scaffold.

Cell culture

Electrospun scaffolds were cut from each aluminium sheet into 1.4 cm diameter circular disks and positioned in 24-well tissue culture plates (Costar, Turin, Italy). They were then incubated in 20% ethanol for 10 min and then extensively washed in sterile phosphate-buffered saline (PBS).

Human bone cells were obtained from explants of cortical mandible bone collected during a surgical procedure from a healthy 66 year-old male subject. The study was approved by the local ethics committee, and informed consent was obtained from the patient. Bone fragments were cultured in Dulbecco's modified Eagle's medium (DMEM)/Ham's F12 medium (1:1) supplemented with 20% fetal bovine serum (FBS), 1% sodium pyruvate, 1% non-essential amino acids, 1% antibiotic/antimycotic solution, 1 U/mL insulin (all from Gibco, Invitrogen, Milan, Italy) until cells migrated from the bone fragments. At confluence the cells were detached with trypsin–EDTA (Gibco) and cultured in complete medium supplemented with 50 μg/mL ascorbic acid, 10 nM dexametasone, and 10 mM β-glycerophosphate (all from Sigma-Aldrich).

At the 5th–8th passage human (*h*)-osteoblasts 2×10^5 cells/well ($\sim 1.3 \times 10^5$ cells/cm^2) in the culturing medium were seeded in 100 μL supplemented complete medium on electrospun matrices and incubated as specified for each experiment in a humidified tissue culture incubator (Heraeus; Corston, Bath, UK) at 37 °C in 5% CO_2 and 95% humidity. The incubator was also equipped with an additional pan of sterile water to prevent evaporation of tissue culture media. The volume and the pH of the complete medium were checked daily.

Biological assays

MTT (3-(4,5-dimethylthiazole-2-yl)-2,5-diphenyl tetrazoliumbromide) assay

Cellular adhesion was assessed using the MTT test. Osteoblasts seeded on electrospun matrices were incubated for 2 h, a time interval previously demonstrated to ensure optimal adhesion of human osteoblasts to functionalized surfaces [17]. At the end of incubation the culture medium and non-adherent osteoblasts were removed. Each well was washed with PBS and incubated with 100 μL of fresh complete medium culture containing MTT (5 mg/mL in PBS, Sigma) at 37 °C for 4 h. The reaction was stopped by adding a sodium dodecyl sulfate (SDS) solution 10% (w/v) acidified with 0.01 N HCl and then stirred for 12 h. To quantify the number of adherent cells, a standard curve was obtained for each experiment by seeding a known number of cells in 24-well tissue culture plates. Cellular lysates (100 μL) were transferred to 96-well plates to determine the absorbance at 620 nm using a microplate reader (Sunrise, Tecan, Milan, Italy).

Calcium assay

The presence of calcium in the wells correlates with osteoblast differentiation and proliferation [18]. To thoroughly optimize the calcium assay protocol, in a separate set of experiments *h*-osteoblasts were seeded onto matrices for 2, 7, and 14 days. The complete culture medium was replaced every 2 days. The calcium content was undetectable at 2 days of incubation, peaked at 7 days, and decreased at 14 days. Osteoblasts were thus cultured onto the scaffold for 7 days. At the end of the incubation period, the culture medium was removed, each well was washed with PBS, and 200 μL of trichloroacetic acid (TCA) 5% (w/v) in PBS were added. Plates were then stirred for 30 min at 4 °C. One hundred microliters was taken from each well, placed in a 96-well-plate and combined with 3.6 mM HCl, 100 μM of *o*-cresolphthalein complexone (Sigma), 0.142 g/mL 2-amino-2-methyl-1-propanol (Sigma) to a final volume of 300 μL, pH 10.7.

A standard curve was obtained by adding all the reagents to the serial dilutions of $CaCO_3$ (from 30 to 0 mg). The absorbance of the purple colored complex was determined using a microplate spectrophotometer at a 620 nm wavelength. The protein concentration was determined using the bicinchoninic acid (BCA) method (Pierce Thermo Scientific, Rockford, IL, USA) in 25 μL of TCA-cell lysate to normalize the calcium levels to the cell density in the different scaffolds.

Quantitative real time polymerase chain reaction (qRT-PCR)

Levels of mRNA transcripts specific for human osteopontin (*hSPP1*), bone sialoprotein (*hIBSP*) and alkaline phosphatase (*hALP*) were measured in osteoblast cells seeded on electrospun scaffolds. Using a SV Total RNA Isolation System kit (Promega, Milan, Italy), total RNA was extracted 24 h after seeding, as described elsewhere [19]. Contaminating DNA was removed by DNase I digestion and 5 μg of total RNA were used to generate randomly primed cDNAs with Moloney Murine Leukemia Virus reverse transcriptase (Applied Biosystems, Milan, Italy). Real time quantitative PCR (qPCR) was performed in an ABI Prism 7700 sequence detector (Applied Biosystems) for 40 cycles at 60 °C annealing temperature. Reactions were performed using TaqMan Universal PCR Master Mix and Universal Probe Library (Roche, Milan, Italy) carrying a fluorescent dye following the manufacturer's instructions. Standard curves were obtained for each gene by amplifying the corresponding cDNAs subcloned into the pGEM-T vector (Promega).

Expression of the target genes was normalized to the endogenous control gene human glyceraldehyde 3-phosphate dehydrogenase (*hGAPDH*). The oligonucleotide primer sequences and probes are listed in Table 2.

Table 2
Oligonucleotide primer sequences.

Gene	Primers sequence	Cycle	Amplicon size (°C)
hSPP1	*Forward*: 5′tttcgcagacctgacatcc3′ *Reverse*: 5′ggctgtcccaatcagaagg3′	40	60
hIBSP	*Forward*: 5′caatctgtgccactcactgc3′ *Reverse*: 5′tcattttggtgattgcttcct3′	40	60
hALP	*Forward*: 5′ggcacctgccttactaactcc3′ *Reverse*: 5′cttagccacgttggtgttga3′	40	60
hGAPDH	*Forward*: 5′cgggaagcccatcacca3′ *Reverse*: 5′ccggcctcaccccatt3′	40	60

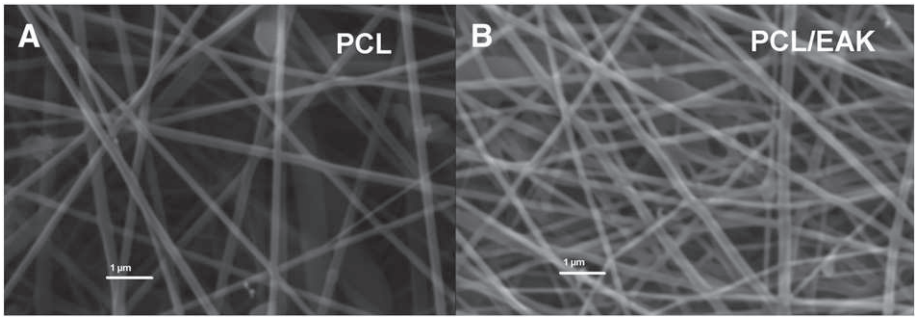

Fig. 1. SEM images of two of the scaffolds investigated at 30,000×. (A) PCL scaffold; (B) PCL-EAK scaffold. The SEM images of the other peptide-enriched samples looked like (B).

Statistical analysis

Statistical analysis was performed using the one-way ANOVA test followed by Bonferroni's multicomparison test with a minimum confidence level of 0.05 for statistical significance. All experiments were performed three times in triplicate. Data are reported as the mean ± standard deviation of the mean.

Results

Morphological characterization

Optimizing the electrospinning parameters made it possible to produce regular fibers without drops as shown in the SEM images (Fig. 1). Appearing randomly distributed, the fibers had diameters falling in the 100–200 nm range.

Surface wettability

Determining the angle of contact between the surface of the matrix and a drop of water made it possible to divide the surfaces into two groups: hydrophobic surfaces ($\theta > 90°$) i.e. the matrices made only with PCL and more hydrophilic surfaces ($\theta < 90°$) i.e. the matrices enriched with peptides (Fig. 2 and Table 3). Interestingly, the addition of a non-self-assembling sequence (RGD-EAKsc) produced the smallest deviation from the PCL value.

Differential scanning calorimetry analysis

PCL matrix

As shown on Fig. 3, a glass transition at $Tg = -63 \pm 1$ °C with a $\Delta Cp = 0.076 \pm 0.02$ J g^{-1} K^{-1} and a melting at $Tonset = 55.2 \pm 0.8$ °C with an enthalpy $\Delta Hm = 53.6 \pm 4$ J/g was observed at the first scan of the PCL matrix recorded at 10 °C/min**.**

These results are in full agreement with the literature data reporting a glass transition between −60 °C and −65 °C and melting at 55.7 °C for polycaprolactone [20]. The crystallinity for PCL was evaluated at $\chi c = \Delta Hm/\Delta H_c^0 = 0.65$, considering that the melting enthalpy of 100% crystalline PCL is 81.6 J/g [21].

PCL/SA peptide matrices

The same analysis was performed for all the samples (Fig. 3) and the results are outlined in Table 4. The glass transition of matrices enriched with peptides was not measurable on the first scan, demonstrating that the peptides constrained the amorphous phase of the polymer. All the samples underwent the glass transition at around −65 °C after the melting (second scan, not shown), as commonly observed in the literature for PCL, but the weaker ΔCp values showed a reduced mobility during the amorphous phase when the peptides were added. As reported in Table 4, the melting temperature—considered as the onset temperature—was lower for all the matrices enriched with peptides compared to the control PCL, while the half-width of the melting endotherm was significantly increased, with apparition of multiple peaks demonstrating a distribution of the crystalline phase. A supplementary DSC experiment was performed at 5 °C/min from 20 °C to 80 °C in order to further investigate the melting zone for all the samples (not shown). In contrast with the control PCL which possessed a single melting endotherm, the matrices enriched with peptides had multiple melting endotherms, with apparition of a higher temperature endotherm corresponding to stabilized crystallites.

Thermally stimulated depolarization currents analysis (TSDC)

The complex TSDC spectra of control PCL, PCL/EAK and PCL/EAbuK performed in triplicate were recorded after a polarization temperature of 20 °C and produced reproducible spectra that are outlined in Fig. 4. Two relaxation modes were observed in this temperature range for the three samples. The first mode was at −56 °C (±1 °C) for all the samples attributed to the dielectric manifestation of the glass transition (PCL). It is noteworthy that the dielectric mode associated with the glass transition was observed for all the samples at the first run, in contrast with DSC analysis, due to the high sensibility of TSDC towards the amorphous phase of polymers. The second mode was observed between 5 °C and 8 °C for the three samples. By analogy with the dielectric behavior of other semi-crystalline polymers, this mode could be either addressed to the glass transition of the constrained amorphous phase or to the polarization phenomenon due to the peculiar architecture of electrospun PCL, in contrast with the first mode, associated to the unconstrained amorphous phase.

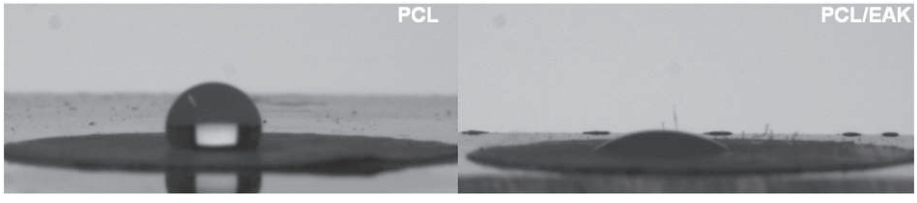

Fig. 2. Contact angle images of two of the scaffolds investigated.

Table 3
Values (means ± SD) of the contact angle determined for each of the different scaffolds.

PCL	PCL/EAK	PCL/DAK	PCL/EAbuK	PCL/EYK	PCL/RGD-EAK	PCL/RGD-EAKsc
114.4° ± 1.8°	34.3° ± 2.0°	57.4° ± 2.5°	49.3° ± 3.1°	76.5° ± 2.1°	70.1° ± 1.9°	86.8° ± 2.2°

This phase is generally called "the rigid amorphous phase," constrained by crystallites, in opposition with the "mobile amorphous phase." In order to attain complementary information on the relaxation processes scanned by DDS, the fractional polarization (FP) method was applied to experimentally resolve the complex TDSC spectra of PCL matrices into elementary spectra. A set of 15 elementary spectra was obtained by shifting the polarization window from −85 °C to −15 °C. Each elementary spectrum obtained by the FP method can be considered a Debye peak, and thus is associated with a single relaxation time τ(T). Using a Bucci–Fieschi framework [22], the temperature dependence of τ(T) can be determined experimentally without any hypothesis about its temperature dependence. In this case the temperature dependence of all the relaxation times isolated by the FP method was found to obey an Arrhenius law:

$$\tau(T) = \tau_0 \exp\left(\frac{Ea}{RT}\right)$$

where R is the gas constant, Ea the activation energy and τ_0 the pre-exponential factor.

The logarithmic variation of the pre-exponential factor *versus* the activation enthalpy is plotted in Fig. 5 for the three matrices. The parameters of the elementary processes associated with the first mode are connected by a linear relationship. Called "the compensation phenomenon," it is largely observed at the dielectric glass transition, revealing the cooperative nature of glass transition with motions of increasing activation energy and entropy [23]. The maximum value of the activation energy is 261 kJ/mol for the control PCL and falls to 207 kJ/mol for the two peptide-enriched matrices. The restricted scale of energy is to be linked to the mobility restriction in the mobile amorphous phase of the matrices enriched with peptides.

XPS analysis

XPS analysis of all the samples investigated showed a N1s signal at 400.0 eV related to the peptide nitrogens. The atomic ratios measured were in agreement with the values that were expected on the basis of the peptide:polymer weight ratio (5:95). Detailed data are reported elsewhere [24].

FT-IR analysis

Due to PCL carbonyl group stretching, the band at 1730 cm^{-1} was present in all FT-IR spectra. Bands typical of peptide bonds were also detected in the hybrid matrices: the amide I band was between 1620 and 1660 cm^{-1}, whereas the amide II band was around 1540 cm^{-1}. The exact position of each band gives information about the secondary structure of the peptide incorporated into the matrix. The amide band position at 1650 cm^{-1} can be attributed to α-helix or random coil structures, whereas the band at 1620–1640 cm^{-1} is indicative of β-sheet structures. An estimation of secondary structure content was obtained utilizing curve fitting analysis. The percent value of β-sheet conformer for each sample is the following: PCL-EAK 89%; PCL-DAK 85%; PCL-EAbuK 90%; PCL-EYK 88%; PCL-RGD-EAK 57%; PCL-RGD-EAKsc 30%.

As expected, treating the RGD-EAK sample with 150 mM NaCl, 10 mM NaH_2PO_4, and pH 7.4 buffer for three days produced a variation in the secondary structure balance (75% β-sheet and 25% α-helix/random coil). A detailed description of the FT-IR analysis is presented elsewhere [24].

Biological assays

Adhesion of *h*-osteoblasts onto hybrid scaffolds was evaluated 2 h after seeding using MTT assay. The cell adhesion onto all the scaffolds enriched with self-assembling peptide was greater than PCL or PCL/

Table 4
Thermal parameters of the amorphous phase of PCL samples from the first thermogram at 10 °C/min, expressed as means ± SD.

Sample	Tg (°C)	ΔC ($J\ g^{-1}\ K^{-1}$)	Tonset (°C)	Half-width (°C)	ΔH (J/g)
PCL	−63 ± 1	0.076 ± 0.02	55.2 ± 0.4	3.0	53.6 ± 4
PCL/EAK	Not meas.	Not meas.	54.2 ± 0.6	5.3	62.6 ± 4.5
PCL/RGD-EAK	Not meas.	Not meas.	53.4 ± 0.4	6.1	53.4 ± 5.7
PCL/RGD-EAK sc	Not meas.	Not meas.	54.0 ± 0.8	5.3	48.2 ± 4.2
PCL/EAbuK	Not meas.	Not meas.	53.1 ± 0.5	6.0	50.4 ± 6
PCL/EYK	Not meas.	Not meas.	53.6 ± 0.7	7.1	42.0 ± 4.8
PCL/DAK	Not meas.	Not meas.	53.4 ± 0.6	7.5	47.6 ± 4.5

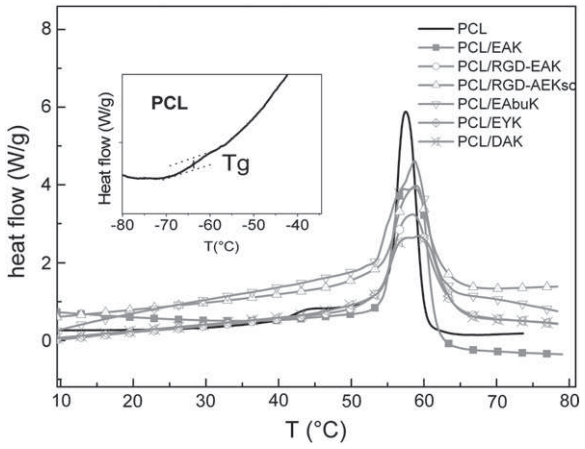

Fig. 3. DSC thermograms of PCL matrices (10 °C/min).

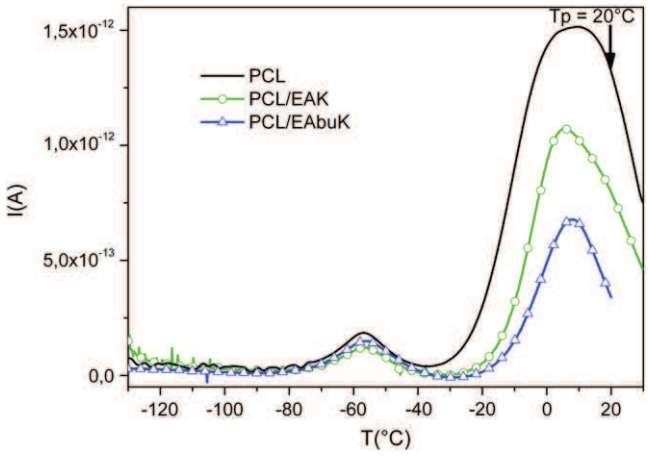

Fig. 4. TSDC spectra of PCL matrices recorded after a polarization at 20 °C.

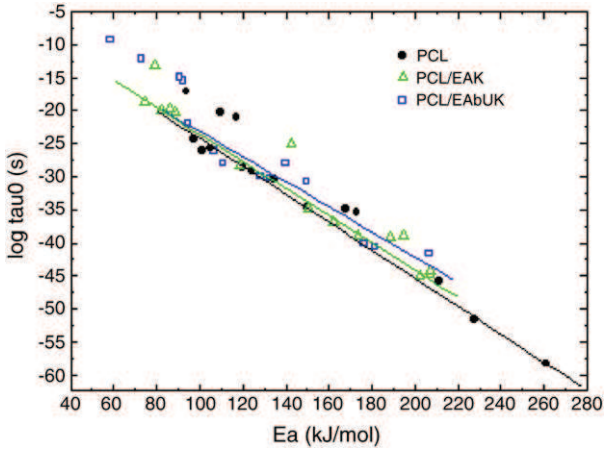

Fig. 5. Variation of the preexponential factor τ_0 versus the activation enthalpy for the elementary relaxation times of PCL matrices.

RGD-EAKsc. The increase with respect to the control (PCL) went from 20% (PCL/EYK) to 90% (PCL/RGD-EAK) (Fig. 6).

The quantity of calcium in the scaffolds was determined through the o-CPC method 7 days after *h*-osteoblast seeding (Fig. 7). The presence of self-assembling peptides in the matrices increased the calcium levels with respect to those in the control (all data are significant with the exception of PCL/EAK). The scaffold enriched with RGD-EAKsc (non-self-assembling sequence) produced results that were similar to the PCL. The best performing sequences were RGD-EAK and EAbuK.

The expressions of *hALP*, *hOPN* and *hBSP* were evaluated through qRT-PCR 24 h after cell seeding. The over expression of *hALP* gene was ascertained for all peptide-enriched scaffolds; a higher increase was registered for cells seeded on PCL/EAbuK (Fig. 8). The level of *hOPN* mRNA remained stable or slightly increased in the cells seeded on PCL/EYK or PCL/EAK, respectively, while it was markedly increased when *h*-osteoblasts were seeded on PCL/DAK, PCL/EAbuK and PCL/RGD-EAK (Fig. 8). Finally *hBSP* expression was higher in the cells cultured on PCL/EAK, PCL/DAK, PCL/EAbuK and PCL/RGD-EAK with respect to that in the absence of self-assembling peptides (PCL) (Fig. 8).

Discussion

Hydrogels constructed from fibril-forming peptides or peptidomimetics are useful as chemically defined extracellular matrices alone or in addition to cytokines or growth factors that could be included in the nanofibrous material or covalently attached to it. SA-peptide hydrogels, in fact, facilitate the slow, stable release of active cytokines [8] modulating protein mobility by both physical hindrance and charge interactions between protein and peptide nanofibers. Several researchers are developing methods to decorate SA-peptide nanofibers with active proteins under mild conditions [25]. Interestingly, scaffolds composed of SA-peptides are able to induce adhesion and proliferation of differentiated cells and also to guide cell differentiation of stem cells. Ozeki M et al. suggested that RAD16, a self-assembling ionic complementary peptide, serves as a matrix for osteogenic differentiation of cocultured bone marrow cells *in vitro* and *in vivo* [26]. On the negative side, hydrogels of SA-peptides have relatively modest moduli of up to about 10 kPa, and thus find application as injectable scaffolds for the treatment of small defects rather than as patches for large ones.

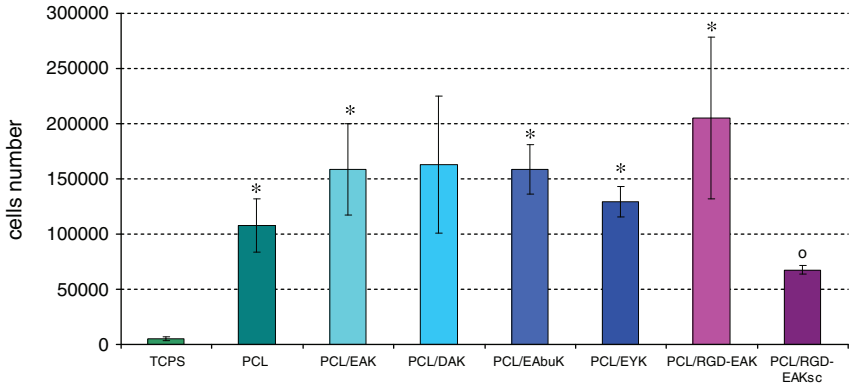

Fig. 6. Adhesion of *h*-osteoblasts onto PCL and peptide-enriched scaffolds evaluated at 2 h after seeding (2×10^5 cells/scaffold). Data were expressed as means ± standard deviation of three independent experiments, each performed in triplicate. * = $p<0.05$ *vs* PCL/RGD-EAK sc, ° = $p<0.05$ *vs* PCL. All data have statistical significance *vs* tissue-culture polystyrene (TCPS).

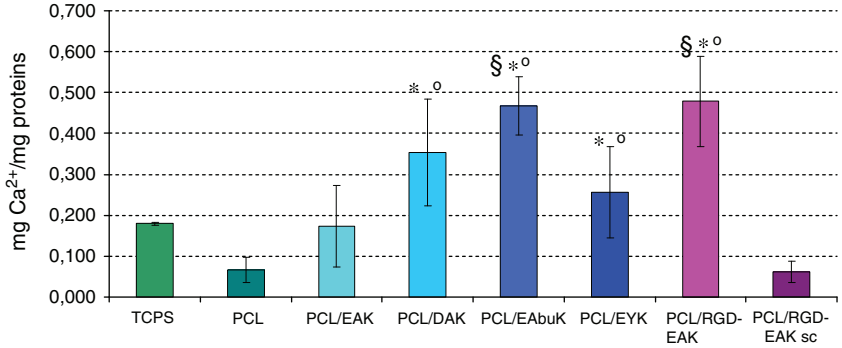

Fig. 7. Quantity of calcium after 7 days after *h*-osteoblast seeding (2×10^5 cells/scaffold) by *o*-CPC method. Data were normalized with bicinchoninic acid assay and expressed as means ± standard deviation of three independent experiments, each performed in triplicate.* $p<0.05$ *vs* PCL/RGD-EAKsc; ° $p<0.05$ *vs* PCL; § $p<0.05$ *vs* TCPS.

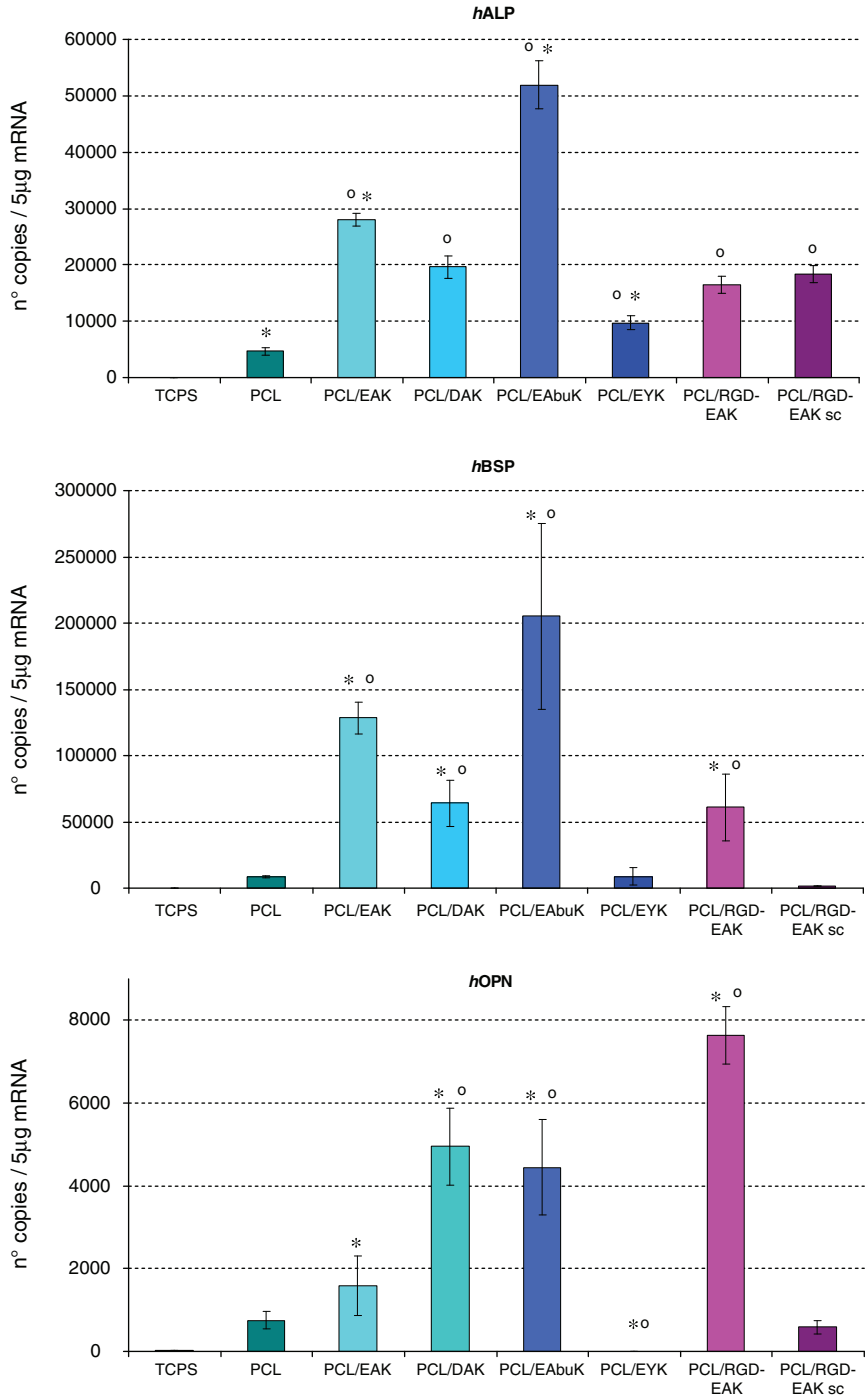

Fig. 8. Evaluation of mRNA transcript levels specific for human alkaline phosphatase (*hALP*), human osteopontin (*hOPN*) and human bone sialoprotein (*hIBSP*) assessed by quantitative real time PCR 24 h after *h*-osteoblast seeding (2×10^5 cells/scaffold). Data are expressed as gene copy number in 5 µg of total RNA. The results were normalized with respect to *hGADPH* (glyceraldehyde-3-phosphate dehydrogenase) and expressed as means ± standard deviation of three independent experiments, each performed in triplicate. All results are significant *vs* TCPS. * $p<0.05$ *vs* PCL/RGD-EAKsc; ° $p<0.05$ *vs* PCL.

With the recent development of the electrospinning process, electrospun nanofibrous scaffolds with large surface area-to-volume ratio, high porosity, and mechanical properties and morphology similar to ECM can be fabricated to serve as ideal bone substitutes [27,28]. While non-biodegradable electrospun polymers such as polyurethane possess substantial mechanical stability, they might interfere with tissue turnover. The ideal scaffold must maintain its stability and promote cell adhesion and growth, but it also needs to degrade gradually as new tissue is being constructed. Electrospun polymers such as PCL, collagen, and gelatin sometimes with the addition of hydroxyapatite, are being investigated by several research groups for bone tissue engineering [29,30]. Although characterized by substantial mechanical stability, PCL is a hydrophobic material, and hydrophobic surfaces generally tend to adsorb larger amounts of proteins such as albumin than do hydrophilic ones [31]. Absorption produces secondary structure changes in proteins considered one of the important aspects affecting blood compatibility [32]. In order to achieve enhanced biocompatibility, some investigators have been focusing on creating a balance between hydrophilic and hydrophobic surface properties [33] or on immobilizing hydrophilic polymers onto hydrophobic surfaces.

In an effort to optimize ECM-mimetic electrospun fiber scaffolds' surface biocompatibility and stiffness, the attempt was made to unite a biodegradable FDA-approved polymer (PCL) with self-assembling peptides in a physiological environment to create nanofibrous structures. This was done with the intention, on the one hand, to remedy PCL's high hydrophobicity and lack of biochemical signals and, on the other, to rectify the excessive softness of peptide hydrogels. Analysis of the scaffolds obtained by electrospinning a solution of self-assembling peptides and PCL in hexafluoroisopropanol (HFIP) showed that:

- the scaffolds presented a fibrous structure with fiber diameters falling in the 100–200 nm range which is comparable with that typical of the extracellular matrix ($180 \pm \%\ 50$) [34];
- enrichment with self-assembling peptides produced a higher water wettability of the scaffold surface. Optimal cell adhesion occurs in moderately hydrophilic substrates while highly hydrophilic or hydrophobic materials hamper cell adhesion [35];
- SA-peptides strongly interacted with the polymer modifying the melting of the hybrid material as revealed by differential scanning calorimetry (DSC). The thermal behaviour of the matrices enriched with peptides cannot be attributed to a simple physical blend. This assumption is corroborated by TSDC experiments providing information on the molecular mobility of the amorphous phases of PCL matrices. The dielectric manifestation of the glass transition associated with the unconstrained, mobile phase implies motions of restricted enthalpy for the matrices enriched with peptides when compared with control PCLs, revealing peptide interactions not only with the crystalline phase of PCL but also with the amorphous one. The lack of any measurable glass transition on DSC thermograms for PCL/SA peptides, moreover, clearly indicates that there has been a stiffening of the PCL matrices that can be linked to enhanced mechanical properties, since literature data show a good correlation between thermal and mechanical behaviors in PCL matrices [36].
- the peptides did not modify their secondary structure after electrospinning maintaining β-sheet conformation that is fundamental for their self-aggregation and consequently for 3D scaffold formation;

Maintaining β-sheet conformation is mandatory for *h*-osteoblast adhesion. As demonstrated by the MTT assay, osteoblasts mainly attach to supports that are very close to the ECM. PCL and PCL/SA peptide matrices thus increased cell adhesion as compared to TCPS and PCL/RGD-EAKsc, a non SA peptide with the lowest β-sheet conformation. It is noteworthy that the comparison between the RGD-EAK and RGD-EAKsc outcomes demonstrated that the enhanced cell adhesion observed was not dependent on the RGD adhesive sequence alone but rather on the presence of the adhesive tripeptide in a well-defined 3D environment. The increase in wettability produced by peptide addition, moreover, demonstrated that cells detect and preferentially adhere to hydrogel fibrous structure. Cell attachment to PCL and PCL/SA peptides led to increased mRNA levels of the bone cell phenotype-related gene alkaline phosphatase, outlining the role of the 3D hydrophilic structure in the maintenance of the osteoblast phenotype. Only PCL/RGD-EAK, PCL/DAK, and PCL/EAbuK, however, specifically increased calcium content and mRNA transcript levels of osteopontin (OPN), the gene coding protein involved in cell attachment to bone-matrix. These data suggest that there is a matrix-specific induction of intracellular signaling that warrants further investigation to understand the function of peptides and indicate that the most interesting ones for the future development of hybrid scaffolds are RGD-EAK and EAbuK.

Conclusions

To summarize, nanofibrous biomimetic scaffolds were developed by mixing PCL with self-assembling peptides. The electrospinning process did not perturb the secondary structure of the self-assembling peptides. Five per cent peptide enrichment produced a higher surface wettability, an amorphous phase constrained by peptides, and enhancement of *h*-osteoblast adhesion to maintain osteoblast differentiation and to stimulate the expression of *hALP*, *hOPN* and *hBSP* genes.

Acknowledgments

The authors would like to thank Dr. Elena Bozza for her assistance in preparing the scaffolds and Dr. Linda Inverso for the review of the manuscript. This work has been in part supported by Grant of the MIUR (PRIN 2005, ex60%2010).

References

[1] Li W, Jiang YJ, Tuan RS. Chondrocyte phenotype in engineered fibrous matrix is regulated by fiber size. Tissue Eng 2006;12:1775-85.
[2] Li WJ, Danielson KG, Alexander PG, Tuan RS. Biological response of chondrocytes cultured in three-dimensional nanofibrous poly(ε-caprolactone) scaffolds. J Biomed Mater Res A 2003;67:1105-14.
[3] Choi JS, Lee SJ, Christ GJ, Atala A, Yoo JJ. The influence of electrospun aligned poly(epsilon-caprolactone)/collagen nanofiber meshes on the formation of self-aligned skeletal muscle myotubes. Biomaterials 2008;29:2899-906.
[4] Venugopal J, Ma LL, Yong T, Ramakrishna S. *In vitro* study of smooth muscle cells on polycaprolactone and collagen nanofibrous matrices. Cell Biol Int 2005;29:861-7.
[5] Ma Z, He W, Yong T, Ramakrishna S. Grafting of gelatin on electrospun poly(caprolactone) nanofibers to improve endothelial cell spreading and proliferation and to control cell orientation. Tissue Eng 2005;11:1149-58.
[6] Yoshimoto H, Shin YM, Terai H, Vacanti JP. A biodegradable nanofiber scaffold by electrospinning and its potential for bone tissue engineering. Biomaterials 2003;24:2077-82.
[7] Li WJ, Tuli R, Okafor C, Derfoul A, Danielson KG, Hall DJ, et al. A three-dimensional nanofibrous scaffold for cartilage tissue engineering using human mesenchymal stem cells. Biomaterials 2005;26:599-609.
[8] Gelain F, Unsworth LD, Zhang S. Slow and substained release of active cytokines from self-assembling peptide scaffolds. J Control Release 2010;145:231-9.
[9] Segers VF, Lee RT. Local delivery of proteins and the use of self-assembling peptides. Drug Discov Today 2007;12:561-8.
[10] Miller RE, Grodzinsky AJ, Vanderploeg EJ, Lee C, Ferris DJ, Barrett MF, et al. Effect of self-assembling peptide, chondrogenic factors, and bone marrow-derived stromal cells on osteochondral repair. Osteoarthritis Cartilage 2010;18:1608-19.
[11] Segers VFM, Tokunou T, Higgins LJ, MacGillivray C, Gannon J, Lee RT. Local delivery of protease-resistant stromal cell derived factor-1 for stem cell recruitment after myocardial infarction. Circulation 2007;116:1683-92.
[12] Misawa H, Kobayashi N, Soto-Gutierrez A, Chen Y, Yoshida A, Rivas-Carrillo JD, et al. PuraMatrix facilitates bone regeneration in bone defects of calvaria in mice. Cell Transplant 2006;15:903-10.
[13] Gambaretto R, Tonin L, Di Bello C, Dettin M. Self-assembling peptides: sequence, secondary structure in solution and film formation. Biopolymers 2008;89:906-15.
[14] Thomas V, Jagani S, Johnson K, Jose MV, Dean DR, Vohra YK, et al. Electrospun bioactive nanocomposite scaffolds of polycaprolactone and nanohydroxyapatite for bone tissue engineering. J Nanosci Nanotechnol 2006;6:487-93.
[15] Gelain F, Panseri S, Antonini A, Cunha C, Donega M, Lowery J, et al. Transplantation of nanostructured composite scaffolds results in the regeneration of chronically injured spinal cords. ACS Nano 2011;5:227-36.
[16] Moulder JF, Stickle WF, Sobol PE, Bomben KD. Handbook of X-ray photoelectron spectroscopy. Eden Prairie: Perkin-Elmer Corp; 1992.
[17] Bagno A, Piovan A, Dettin M, Brun P, Gambaretto R, Palù G, et al. Improvement of Anselme's adhesion model for evaluating human osteoblast response to peptide-grafted titanium surfaces. Bone 2007;41:704-12.
[18] Ortiz J, Chou LL. Calcium upregulated survivin expression and associated osteogenesis of normal human osteoblasts. J Biomed Mater Res A 2012;100:1770-6.
[19] Brun P, Ghezzo F, Roso M, Danesin R, Palù G, Bagno A, et al. Electrospun scaffolds of self-assembling peptides with poly(ethylene oxide) for bone tissue engineering. Acta Biomater 2011;7(6):2526-32.
[20] Polo Fonseca C, Cavalcante F, Amaral FA, Zani Souza CA, Neves S. Thermal and conduction properties of a PCL-biodegradable gel polymer with $LiClO_4$, LiF_3CSO_3, and $LiBF_4$ salts. Int J Electrochem Sci 2007;2:52-63.
[21] Gummow RJ, de Kock A, Thackeray MM. Improved capacity retention in rechargeable 4 V lithium/lithium–manganese oxide (spinel) cells. Solid State Ionics 1994;69:59-67.
[22] Bucci C, Fieshi R, Guidi G. Ionic thermocurrents in dielectrics. Phys Rev 1966;148:816-33.
[23] Samouillan V, Dandurand J, Lacabanne C, Hornebeck W. Molecular mobility of elastin: effect of molecular architecture. Biomacromolecules 2002;3:531-7.
[24] Iucci G, Ghezzo F, Danesin R, Modesti M, Dettin M. Biomimetic peptide-enriched electrospun polymers: a photoelectron and infrared spectroscopy study. J Appl Polym Sci 2011;122:3574-82.
[25] Mahmoud ZN, Gunnoo SB, Thomson AR, Fletcher JM, Woolfson DN. Biorthogonal dual functionalization of self-assembling peptide fibers. Biomaterials 2011;32:3712-20.

[26] Ozeki M, Kuroda S, Kon K, Kasugai S. Differentiation of bone marrow stromal cells into osteoblasts in a self-assembling peptide hydrogel: *in vitro* and *in vivo* studies. J Biomater Appl 2011;25:663-84.
[27] Chapekar MS. Tissue engineering: challenges and opportunities. J Biomed Mater Res 2000;53:617-20.
[28] Li WJ, Laurencin CT, Caterson EJ, Tuan RS, Ko FK. Electrospun nanofibrous structure: a novel scaffold for tissue engineering. J Biomed Mater Res 2002;60:613-21.
[29] Singh S, Ray SS. Polylactide based nanostructured biomaterials and their applications. J Nanosci Nanotechnol 2007;7:2596-615.
[30] Prabhakaran MP, Venugopal J, Ramakrishna S. Electrospun nanostructured scaffolds for bone tissue engineering. Acta Biomater 2009;5:2884-93.
[31] Luensmann D, Jones L. Albumin adsorption to contact lens materials: a review. Cont Lens Anterior Eye 2008;31:179-87.
[32] Yan H, Xiaoying L, Jinwu M, Nan H. *In vitro* investigation of protein adsorption and platelet adhesion on inorganic biomaterial surfaces. Allied Surf Sci 2008;255: 257-9.
[33] Wang YX, Robertson JL, Spillman WB, Claus RO. Effects of the chemical structure and the surface properties of polymeric biomaterials on their biocompatibility. Pharm Res 2004;21:1362-73.
[34] Tzaphlidou M. The role of collagen in bone structure: an image processing approach. Micron 2005;36:593-601.
[35] Bacakova L, Filova E, Parizek M, Ruml T, Svorcik V. Modulation of cell adhesion, proliferation and differentiation on materials designed for body implants. Biotechnol Adv 2011;29:739-67.
[36] Williamson MR, Coombes AGA. Gravity spinning of polycaprolactone fibres for applications in tissues engineering. Biomaterials 2004;25:459-65.